Electrochemical aspects of the generation of ramified metallic electrodeposits

J.-N. Chazalviel
Laboratoire de Physique de la Matière Condensée, Ecole Polytechnique, F-91128 Palaiseau, France
(Received 16 July 1990)

The growth of ramified metallic deposits by electrodeposition from dilute salt solutions and in a high electric field has been considered in the geometry of a thin rectangular cell. The equations governing ion motion in the case of a dilute electrolyte have been solved numerically and analytically in a one-dimensional (1D) and a 2D approximation. It is found that ramified growth is a direct consequence of the creation of a space charge upon anion depletion in the vicinity of the cathode. The front of the ramified deposit is predicted to advance at a speed just equal to the velocity of the anions in the applied electric field. The presence of this space charge ahead of the growing front is associated with a potential drop δV. Resolution of the equations in the 2D case shows that the dense-parallel morphology of the deposit also results quite naturally from the existence of a space charge in the vicinity of the filament tips. The average filament spacing and sidebranch tilting angle can be directly related to the values of δV and of the applied electric field. The mechanism giving rise to the space charge will apply as well to any physical system involving electric conduction with two types of carriers, if one of them exhibits blocking-contact characteristics.

I. INTRODUCTION

The recent activity in the field of fractals and diffusion-limited aggregation (DLA) has brought renewed interest in the old subject of "dendritic" electrodeposition of metals from a salt solution. Under certain conditions, i.e., in the presence of a supporting electrolyte and in a restricted potential range, the motion of the metal cations is indeed solely governed by diffusion, and the electrodeposition process is then expected to be well described by DLA. However, this process is very slow[1,2] and is complicated by recrystallization phenomena. A much more efficient way for producing ramified structures by electrodeposition consists in taking a dilute solution of a pure salt, e.g., 10^{-3} M to 10^{-1} M $CuSO_4$ or $ZnSO_4$ (i.e., without supporting electrolyte), and applying a large potential (~ 10 V) between two electrodes dipped in the solution.[3-9] Fractal-like structures can then be grown at speeds as high as ~ 1 mm/s.

Most recent efforts have focused on the geometrical aspects of the problem, various morphologies of the aggregates have been identified, depending upon the experimental conditions ("DLA-type," "dense branching," etc.) and fractal dimensions have been measured. However, the basic electrochemical aspects of the problem have been little considered in the context of these studies. On the other hand, while the electrochemical literature has largely addressed the problem of roughening in electrodeposition,[1,10-13] the present case of simple binary electrolytes has been usually avoided in these studies, as it is of lesser technological interest, and there is general agreement that the absence of a supporting electrolyte causes departures from electroneutrality and breakdown of the standard framework of diffusion-limited ion transport, hence raising considerable theoretical difficulties. However, the central problem of electroneutrality near an electrode has been questioned on more general grounds, especially by Newman, and an expansion approach to this problem has been proposed.[14-16] We feel yet that the problem is far from being settled, so that the fundamental question on the respective roles of diffusion and electromigration in "fractal" electrodeposition experiments remains largely unanswered. We will try to address this question in the following.

We will consider the growth of metal electrodeposits in a two-dimensional geometry, starting from a linear cathode. In Sec. II we will calculate the distribution of electrostatic potential and ion concentrations for a dilute electrolyte, in the hypothetical case where uniform (nonramified) electrodeposition would take place. A simple solution may be derived. The paradoxical result that is obtained will prompt a critical revision of the hypotheses. This will lead us to the conclusions that the ramified growth is initiated by the creation of a very large electric field near the interface, and that the velocity of the front of the deposit is determined by the *velocity of the anions.* This theoretical prediction has been verified experimentally and some preliminary results have been reported elsewhere.[17] In Sec. III we will consider the regime of "dense-parallel" electrodeposition and try to understand what the origin of the characteristic length that determines the spacing between the growing filaments is. It will be shown that it comes out simply from the basic equations of ion migration.

II. THEORY FOR THE UNIFORM-DEPOSITION CASE

A. The basic equations

We consider a thin rectangular cell, as sketched in Fig. 1. We assume that the two electrodes are made of the same metal, and that the cell is filled with a dilute solution of a salt of this metal (soluble anode cell). The motion of the ions is described by concentration-independent mobilities (μ_c for the cations, μ_a for the

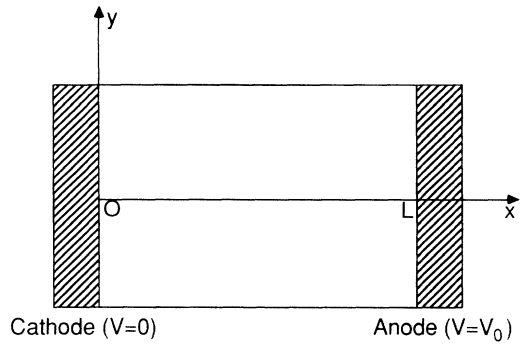

FIG. 1. Scheme of the cell.

anions) and diffusion constants (respectively D_c and D_a), which is a reasonable approximation for very dilute solutions.[18] We neglect convection of the electrolyte, which is reasonable to some extent for a very thin cell. The basic equations for the concentrations C_c and C_a are then

$$\frac{\partial C_c}{\partial t} = -\nabla \cdot \mathbf{W}_c \ , \tag{1}$$

$$\frac{\partial C_a}{\partial t} = -\nabla \cdot \mathbf{W}_a \ , \tag{2}$$

$$\mathbf{W}_c = -D_c \nabla C_c + \mu_c C_c \mathbf{E} \ , \tag{3}$$

$$\mathbf{W}_a = -D_a \nabla C_a - \mu_a C_a \mathbf{E} \ , \tag{4}$$

where $\mathbf{E}$ is the electric field, and $\mathbf{W}_c$ ($\mathbf{W}_a$) is the cation (anion) flux. The electric current density is given by $\mathbf{J} = z_c e \mathbf{W}_c - z_a e \mathbf{W}_a$, where $z_c e$ and $-z_a e$ are the cation and anion electric charge, respectively. The electrostatic charge density is $\rho = e(z_c C_c - z_a C_a)$ (for the bulk, equilibrium electrolyte, we define $C_0 = z_c C_c^{\text{equ}} = z_a C_a^{\text{equ}}$) and the Poisson equation for the electrostatic potential V can be written

$$\Delta V = -\nabla \cdot \mathbf{E} = -\rho/\epsilon\epsilon_0 = -e(z_c C_c - z_a C_a)/\epsilon\epsilon_0 \ , \tag{5}$$

where ϵ_0 is vacuum permittivity, and ϵ is the dielectric constant of water. Eliminating the fluxes $\mathbf{W}_c$ and $\mathbf{W}_a$, the evolution of the system is fully determined by

$$\frac{\partial C_c}{\partial t} = D_c \Delta C_c - \mu_c \mathbf{E} \cdot \nabla C_c - \mu_c C_c \nabla \cdot \mathbf{E} \ , \tag{6}$$

$$\frac{\partial C_a}{\partial t} = D_a \Delta C_a + \mu_a \mathbf{E} \cdot \nabla C_a + \mu_a C_a \nabla \cdot \mathbf{E} \ , \tag{7}$$

$$\nabla \cdot \mathbf{E} = e(z_c C_c - z_a C_a)/\epsilon\epsilon_0 \ . \tag{8}$$

Let us now consider the hypothetical case where the electrodeposition would be uniform. Then the only relevant space coordinate is x, the electric field becomes a scalar, and Eqs. (6)–(8) reduce to[19]

$$\frac{\partial C_c}{\partial t} = D_c \frac{\partial^2 C_c}{\partial x^2} - \mu_c E \frac{\partial C_c}{\partial x} - \mu_c C_c \frac{\partial E}{\partial x} \ , \tag{9}$$

$$\frac{\partial C_a}{\partial t} = D_a \frac{\partial^2 C_a}{\partial x^2} + \mu_a E \frac{\partial C_a}{\partial x} + \mu_a C_a \frac{\partial E}{\partial x} \ , \tag{10}$$

$$\frac{\partial E}{\partial x} = e(z_c C_c - z_a C_a)/\epsilon\epsilon_0 \ . \tag{11}$$

Now, since the electrolyte is very dilute (cation concentration much smaller than atomic density in the metal) one may assume that the electrodeposition will not significantly affect the size and shape of the electrodes, i.e., the cathode will be fixed at $x=0$ and the anode will be fixed at $x=L$, and the only thing left is to define the boundary conditions at $x=0$ and $x=L$. We suppose that the only electrochemical reactions are metal deposition at the cathode and metal dissolution at the anode, and we assume that the electrochemical kinetics are ideally fast, hence the boundary conditions for the cations are just the conditions for electrochemical equilibrium at the interface, i.e.,[20] $V(0) = -(kT/z_c e)\ln[z_c C_c(0)/C_0]$ and $V(L) = V_0 - (kT/z_c e)\ln[z_c C_c(L)/C_0]$. Since the anions are not involved in the electrochemical reactions, the boundary conditions for the anions are $W_a(0) = W_a(L) = 0$. We will first show that this set of equations and boundary conditions can be solved analytically by using a regional approximation, next we will present the results of a numerical resolution, then we will discuss the consequences for the electrodeposition mechanism.

B. Analytic resolution

If we limit our interest to the steady-state regime, Eqs. (9)–(11) reduce to

$$D_c \frac{d^2 C_c}{dx^2} + \mu_c \frac{d}{dx}\left[C_c \frac{dV}{dx} \right] = 0 \ , \tag{12}$$

$$D_a \frac{d^2 C_a}{dx^2} - \mu_a \frac{d}{dx}\left[C_a \frac{dV}{dx} \right] = 0 \ , \tag{13}$$

$$d^2 V/dx^2 = -e(z_c C_c - z_a C_a)/\epsilon\epsilon_0 \ . \tag{14}$$

Since $W_a(0) = W_a(L) = 0$, the anions in the steady state will simply be in equilibrium in the potential, and Eq. (13) can readily be integrated to

$$W_a = -D_a dC_a/dx + \mu_a C_a dV/dx = 0 \tag{15}$$

or, by using the Einstein relation $D_a/\mu_a = kT/z_a e$,

$$C_a(x) \propto \exp[z_a e V(x)/kT] \ . \tag{16}$$

In the same way, Eq. (12) can be integrated to

$$W_c = -D_c dC_c/dx - \mu_c C_c dV/dx = J/z_c e \ , \tag{17}$$

where J is the electric current density through the system ($J < 0$). Now a simple solution can be derived by using a regional approximation. In the following, we will be led, quite naturally, to distinguishing two different regions: a quasineutral region ($z_c C_c \approx z_a C_a$) extending from the anode to the vicinity of the cathode, and a space-charge region ($C_a \ll C_c$) in the close vicinity of the cathode.

1. *Region I: the quasineutral region*

The electrostatic potential varies from nearly zero at $x=0$ to about V_0 at $x=L$. Equation (16) tells us that the

anions will be concentrated near the maximum of $V(x)$. As we do not expect a strong concentration of anions (much larger than C_0) over a narrow x range, this indicates that the maximum of $V(x)$ will be rather flat, that is $V(x)$ will stay within $\sim kT/e$ from V_0 in a sizeable part of the cell. [This argument, which is derived from Eq. (16), will of course hold true only for the steady state.] The flatness of $V(x)$ requires a quasineutrality, that is $z_c C_c \approx z_a C_a$, and extracting dV/dx from Eq. (15) and replacing into Eq. (17) reduces the system to

$$\frac{dV}{dx}=\frac{kT}{z_a e C_a}\frac{dC_a}{dx} , \tag{18}$$

$$\frac{-J}{z_c e}=D_c\frac{dC_c}{dx}+\frac{\mu_c C_c}{\mu_a C_a}D_a\frac{dC_a}{dx}=\left[1+\frac{z_c}{z_a}\right]D_c\frac{dC_c}{dx} . \tag{19}$$

Introducing a constant x_I and using J as a parameter that will be determined later, we get

$$z_c C_c = z_a C_a = \frac{-J(x-x_I)}{eD_c(1+z_c/z_a)} , \tag{20}$$

$$V=V(L)+\frac{kT}{z_a e}\ln\frac{x-x_I}{L-x_I} . \tag{21}$$

This region will extend for values of x decreasing from L to some position x_I.

2. *Region II: the space-charge region*

Equation (21) shows that for x_I, the potential becomes markedly smaller than V_0. In this region, according to Eq. (16), C_a will become negligible ($C_a \ll C_c$). There will then remain a space charge $z_c e C_c$, and the potential will be given by

$$d^2V/dx^2=-ez_c C_c/\epsilon\epsilon_0 . \tag{22}$$

Now the current is still given by the two terms in Eq. (17). As we may expect that Eq. (22) will lead to very large electric fields, we will keep only the drift term, as it is expected to be dominant over the diffusion term

$$-J/z_c e=\mu_c C_c dV/dx . \tag{23}$$

Combining Eqs. (22) and (23), we get

$$-\frac{ez_c C_c}{\epsilon\epsilon_0}=\frac{d^2V}{dx^2}=\frac{d}{dx}\left[\frac{-J}{z_c e\mu_c C_c}\right]=\frac{J}{z_c e\mu_c}\frac{1}{C_c^2}\frac{dC_c}{dx} . \tag{24}$$

Integrating the differential equation in C_c yields

$$C_c=\left[\frac{-\epsilon\epsilon_0 J}{2z_c^2 e^2\mu_c(x_I'-x)}\right]^{1/2} , \tag{25}$$

$$V=V_0'-\frac{2}{3}\left[\frac{-2J}{\epsilon\epsilon_0\mu_c}\right]^{1/2}(x_I'-x)^{3/2} , \tag{26}$$

where the constants V_0' and x_I' must be chosen close to $V(L)$ and x_I, respectively, in order to match with region I. Region II will then extend from $x\sim x_I$ down to zero.

3. *Matching at the boundaries*

The values of J and x_I can now be derived from the known quantities. The matching between the two regions has already been used in Eqs. (25) and (26). We are left with the matching of V in $x=0$; from Eq. (26) it gives

$$-x_I^3 J=\{3[V(L)-V(0)]/2\}^2\epsilon\epsilon_0\mu_c/2 . \tag{27}$$

Also we have to express that the total amount of anions in the cell has not changed. This is obtained by integrating C_a from x_I to L in Eq. (20), hence,

$$\frac{-J}{eD_c(1+z_c/z_a)}\frac{(L-x_I)^2}{2}=C_0 L . \tag{28}$$

An order-of-magnitude estimate, taking $D_c=D_a=10^{-5}$ cm^2/V s, $z_c=z_a=1$, $C_0=6\times10^{18}$ cm^{-3} (0.01M), $V_0=10$ V, and $L=1$ cm, gives $-J=40$ μA/cm^2, $x_I=20$ μm, $V_0-V(L)=0.02$ V, and $V(0)=0.3$ V. This shows that one has $x_I \ll L$, $V(L)-V(0)=9.68$ V$\approx V_0$, and the regional approximation is justified. The essential formulas derived above can now be simplified and are summarized hereafter:

$$J=\frac{-2eD_c C_0}{L}(1+z_c/z_a) , \tag{29}$$

$$x_I=\left[\frac{9\epsilon\epsilon_0 L V_0^2}{16kTC_0}\frac{z_c z_a}{z_c+z_a}\right]^{1/3} , \tag{30}$$

$$V(0)=\frac{kT}{z_c e}\ln\left[\frac{3L^2e^3V_0C_0}{4\epsilon\epsilon_0(kT)^2}\left[\frac{z_c z_a}{z_c+z_a}\right]^2\right] , \tag{31}$$

$$V(L)=V_0-(kT/z_c e)\ln 2 ; \tag{32}$$

Region I, $x_I < x < L$:

$$z_c C_c = z_a C_a = 2C_0(x-x_I)/L , \tag{33}$$

$$V=V(L)+\frac{kT}{z_a e}\ln\frac{x-x_I}{L} ; \tag{34}$$

Region II, $0 < x < x_I$:

$$C_a \ll C_c=\left[\frac{\epsilon\epsilon_0 kTC_0}{L(z_c e)^2(x_I-x)}\frac{z_c+z_a}{z_c z_a}\right]^{1/2} , \tag{35}$$

$$V=V(0)+[V(L)-V(0)][1-(1-x/x_I)^{3/2}] . \tag{36}$$

It is interesting to notice that there are several natural lengths in the problem, namely, the length of the cell L, the Debye screening length $\lambda=\{\epsilon\epsilon_0 kT/[e^2C_0(z_c+z_a)]\}^{1/2}$, and the backstream diffusion length $\lambda_b \sim D_c/(\mu_c V_0/L)=L(kT/z_c e)/V_0$ (typically $L\sim1$ cm, $\lambda\sim30$ Å, $\lambda_b\sim100$ μm). This may allow one to get more physical insight into the above parameters. The length x_I is simply of the order of $L(\lambda/\lambda_b)^{2/3}\sim10$ μm. The concentration in region II is roughly $C_c\sim C_0\lambda/[(x_I-x)L]^{1/2}$, which is of the order of $C_0(\lambda^2\lambda_b)^{1/3}/L$ [in order of magnitude, $(\lambda^2\lambda_b)^{1/3}/L\sim10^{-5}$]. These behaviors can be qualitatively understood as a simple consequence of Poisson equation and current conservation: the current is limited by diffusion in the quasineutral re-

gion, i.e., $J \sim eD_c C_0/L$, which is *very small;* the space-charge region must satisfy the Poisson equation ($eC_c^{\text{reg.II}} x_I^2/\epsilon\epsilon_0 \sim V_0$) which makes x_I *small,* and current conservation ($J \sim C_c^{\text{reg.II}} e\mu_c V_0/x_I$) in turn makes $C_c^{\text{reg.II}}$ *small.*

4. *Remark on the boundary conditions: the double-layer regions*

In the preceding we have implicitly neglected what occurs in the immediate vicinity of the interfaces. Actually, there is a sharp variation of electrostatic potential near the interface[20] of magnitude $U_{PZC} - U_{equ}$, where U_{PZC} is the electrode potential corresponding to zero charge, and U_{equ} is the electrode potential corresponding to electrochemical equilibrium. This sharp variation of the electrostatic potential takes place in the so-called "double-layer" region, whose thickness is of the order of the Debye screening length. This is quite short near the anode ($\lambda \sim 30$ Å) but might be appreciably larger near the cathode, since the concentration of the electrolyte is considerably decreased in region II. Also, special conditions may result from the presence of the very large space-charge electric field. If one tries to include the double layers explicitly in the calculation, then V must be taken continuous through the interface, and the boundary condition becomes

$$z_c C_c(0) = C_0 \exp[z_c e(U_{PZC} - U_0)/kT] , \tag{37}$$

where U_0 is the electrode potential corresponding to electrochemical equilibrium in an electrolyte with a cation concentration C_0/z_c.[20] If such a condition is used as the boundary condition at $x = 0$, then a third region appears at very small x values. This characteristic length occurs when dC_c/dx becomes large enough, so that the diffusion term in Eq. (17) competes with the drift term. Taking the surface electric field from Eq. (26) with $x = 0$, this occurs for $x < x_{II} = D_c/(\mu_c dV/dx) = (-\epsilon\epsilon_0 kTD_c/2Jz_c e x_I)^{1/2}$, hence

$$x_{II} = \left[\frac{\epsilon\epsilon_0 L (kT)^2}{6(z_c e)^3 V_0 C_0} \frac{z_c z_a}{z_c + z_a} \right]^{1/3}$$

$$\sim (\lambda^2 \lambda_b)^{1/3} \sim 10^3 \text{ Å} . \tag{38}$$

In spite of the increased value of x_{II} as compared to λ, it is still much smaller than x_I. This justifies having neglected the diffusion term in Sec. II B 2. It also shows that it is quite reasonable to take into account the double layer just as a boundary condition. One will notice, however, that the boundary conditions as given above (Sec. II A) are not complete, since only one condition has been given for C_c and V. If the double layer were included in the system, one would have two conditions [continuity of V and Eq. (37)]. When the double layer is taken outside the system, one may add to the condition of quasiequilibrium (Sec. II A) a condition stating that the diffusion term is negligible. A convenient way of doing so is to take $dC_c/dx = 0$. This condition will be used in the numerical calculation (and we will keep dropping the constant term $U_{PZC} - U_0$, as it has been done above).

C. Numerical resolution

The surprising character of the above results has prompted us to perform a numerical resolution of Eqs. (9)–(11). This was expected to provide a verification of the regional approximation scheme, together with an exact picture of the functions $C_c(x)$, $C_a(x)$, and $V(x)$. Also, such a calculation may provide access to the transient regime, which has not been considered yet. However, for practical display purposes as well as for ease of computation, conditions had to be chosen such that the characteristic lengths in the problem (L, λ, λ_b) do not differ by many orders of magnitude. For this reason, we have been using unrealistically small values for C_0 (10^9–10^{11} cm^{-3}). This is of no trouble since the magnitude of the relevant parameters for the practical concentration range are given by the analytic treatment.

The set of equations (9)–(11) with the boundary conditions has been solved on a microcomputer. The x variable was discretized using a mesh δx and a typical number of 100 mesh points. Starting from a uniform distribution of anions and cations ($\rho = 0$), and a potential $V = V_0 x/L$, the evolution of C_c and C_a was deduced from Eqs. (9) and (10) by applying successive small time increments δt. At each step the Poisson equation (11) was integrated with due care to the boundary conditions on V, and the new potential was used for the next step. The use of an "explicit" recursion scheme in the discretization of (9) and (10) requires, as usual, a stability condition $\delta t < K \delta x^2$ to be fulfilled, where K is some constant depending upon the various coefficients entering the equations.[21]

Typical results for the steady state are shown in Fig. 2. These results are in good agreement with the predictions from the analytic resolution: the concentrations are identical and vary linearly with x in the main part of the cell, while V is essentially constant $V \approx V_0$. In the vicinity of the cathode, a fast variation of V occurs, associated with a small value of C_c and a negligible value of C_a. The thickness of the space-charge layer and the value of C_c in

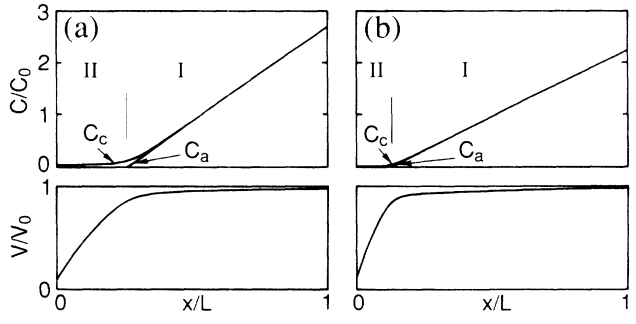

FIG. 2. Profile of the ion concentrations C_c and C_a, and of the electrostatic potential V resulting from the numerical simulation in the hypothetical case of uniform deposition with negligible growth of the cathode. $L = 1$ cm, $V_0 = 1$ V, $D_c = D_a = 10^{-5}$ cm^2/s, $z_c = z_a = 1$, $\epsilon = 80$; (a) $C_0 = 10^{10}$ cm^{-3}, (b) $C_0 = 10^{11}$ cm^{-3}. Notice the two regions I and II as discussed in the text.

this region are found to agree quantitatively with the analytic results, and also exhibit the expected dependence upon changing C_0 (see Fig. 2). In summary, the steady-state regime—in the hypothetical case of uniform deposition—exhibits a squeezing of the applied field in the near-cathodic region. Furthermore, since most of the cell is outside the electric field region, the electrical current in the steady state will be of the order of eD_cC_0/L, an extremely small value, *independent of the applied potential.*

D. Discussion

The steady state described above is actually unphysical: ion motion is governed by diffusion in region I, which occupies the larger part of the cell, and by electric-field migration in region II, i.e., very close to the electrode. This behavior is strikingly different from that encountered in standard electrochemical situations, i.e., with a supporting electrolyte. Also, there is no evidence, among "fractal electrodeposition" experiments, of a system exhibiting a current density independent of the applied potential. Actually, the absurdity of our result was our initial motivation for doing an analytic *and* a numerical calculation. The remarkable agreement between both is a good check of the resolution procedure. Notice also that this is an essentially *exact* solution, in contrast to the expansion methods that have been proposed in the literature.[14] A similar solution for the special case $z_c=z_a=1$ has been recently obtained by Bruinsma and Alexander.[22] Of course, since practical systems behave differently, it will be of uttermost importance to discuss our hypotheses in order to resolve the paradox. However, before going to this discussion, a better understanding of the underlying physics may be gained by looking at the time evolution leading to the steady state in this simple model.

Since the Poisson equation was integrated at each time step in the numerical calculation, the intermediate results give an exact picture of the actual path toward the steady state. Figure 3 shows the graphs of C_c, C_a, and V, at different times, for a typical calculation. At $t=0$, there is no space charge and the field is uniform. The cations then migrate from the anode to the cathode. The cation concentration is not strongly disturbed at the boundaries, since the electrodes can freely absorb or provide cations. The situation for the anions is much more dramatic, because they cannot be transferred to or from the electrodes. So there is a piling up of anions near the anode, and a depleted region near the cathode, whose thickness tends to increase with a velocity $v_a=\mu_a V_0/L$. This tends to create space charges near the electrodes, hence a modification of the potential through the Poisson equation. The problem yet *is not symmetric:* near the anode, the piling up of anions will tend to increase the local field, leading to fast neutralization by an increased arrival of cations from the anode; on the other hand, near the cathode the increased field will only accelerate the cations on their way to electrodeposition. By virtue of current conservation, increased ion speed implies reduced concentration, hence the space charge z_ceC_c will be decreased [actually by a factor $\sim L/(\lambda^2\lambda_b)^{1/3}\sim 10^5$], but

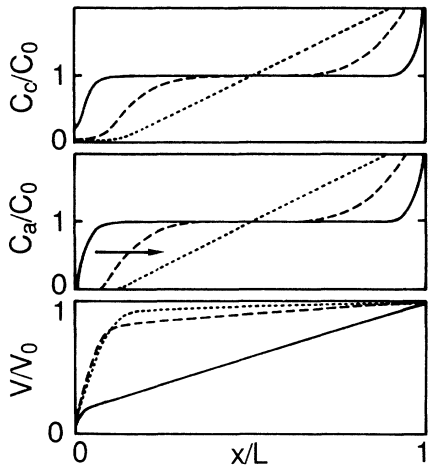

FIG. 3. Profile of the ion concentrations and electrostatic potential as a function of time, for the same system as Fig. 2(b); $t=100$ s (solid lines), $t=10^3$ s (dashed lines), $t=10^4$ s (dotted lines). Notice the motion of the anion distribution, due to the drift in the applied electric field, and the associated rise of the space charge near the cathode.

complete neutralization is unattainable as long as there is a flux of cations to the cathode. The steady-state potential distribution is almost reached when all the potential drop occurs near the cathode. This takes place on a rather fast time scale ($x_I/v_a\sim 1$ s). The steady state for the concentrations takes somewhat longer to attain, as it needs diffusion through the large distance L (and $L^2/D_a\sim 10^5$ s).

Observing the early steps of the evolution therefore shows that the crucial mechanism for the creation of the space-charge region near the cathode is anion migration in the applied electric field. Now it is known that such a steady state will not be obtained in practical systems. The reason for that is also clear from the above: the interface will hardly withstand a potential drop of ~ 10 V over 10 μm. There are various ways in which the system can escape this unphysical situation, thereby violating our simple hypotheses. One is convective motion of the solution. This can be brought about, either if external stirring is provided, or simply under the influence of concentration gradients and gravity,[23] or else under the influence of the current (electroconvection).[22] In all cases, this will provide mixing of the concentrations, which may hinder building of the space charge. However, it is not clear that convection plays a large role in practical experiments (the thin-cell geometry is rather unfavorable for convection, and similar experiments have been realized in media where convection is severely inhibited, such as filter paper).[7] On the other hand, if convection is inhibited, as soon as the interface electric field reaches some critical value, a surface instability may develop: a growing tip will find an increased electric field near its apex, hence an increased deposition rate and a fast growth of the tip, as long as the apex stays in the space-charge region. This mechanism provides a natural explanation for ramified growth, and leads us to some

predictions on the practical behavior. The potential distribution should start to evolve until some potential drop occurs in the nascent space-charge region (this might take a time $\sim x_I/v_a \sim 1$ s), then ramified growth should start. The forward front of the ramified deposits should follow the migrating anions, in such a way that no large space charge can further develop. If the experiment is realized at a *constant current density* J rather than at constant potential, then the front of the deposit should advance at a *constant speed* $v_a = -\mu_a E$, and the potential drop across the cell is expected to follow a law $V = \delta V - E(L - v_a t)$, where E is the (constant) electric field in the neutral region $[J = eC_0(\mu_c + \mu_a)E]$ and δV is the critical potential drop necessary for growing the interface ramified (it is recalled that E and J are negative with our conventions).

These predictions have been verified experimentally for a wide range of experimental conditions: current density, salt concentration, and cell geometry. Especially, the surprising prediction that the velocity of the front is exactly equal to the *anion* velocity in the applied electric field has been verified by using different salts with common cation. A preliminary report on this work has been published elsewhere[17] and a more detailed report is planned to appear later on.[24] The central role of space charge and electric-field migration, evidenced by our calculation and confirmed by these experiments, is at variance with simple guesses, such as those found in the literature.[9]

III. TOWARD AN UNDERSTANDING OF THE MORPHOLOGY

The above calculation has been used as an *ab absurdo* argument. It is of course important now to determine what the actual distributions are during the growth of the ramified electrodeposit. Also, the front of the deposit is probably the most obvious characteristic feature that one may think of, but one may wish to go one step further in the understanding of the morphology. Depending upon the experimental conditions, deposits have been observed to exhibit a branched, treelike, structure, very reminiscent of DLA (this usually takes place at lower fields) or look like a bunch of parallel filaments. This last morphology has been called "dense-branching morphology" ("dense radial" when starting from a point cathode,[4,5] or "dense parallel" when starting from a linear cathode,[17] as it is the case here). In spite of their similar appearance on a microscopic scale, these morphologies are clearly distinct and have attracted much attention, but the reason for this change of behavior is as yet not understood. In the following we will focus on the dense-parallel morphology and will try to analyze the distributions of concentrations and potential during the growth, in order to understand how the invoked instability can give rise to such regular structures, with special attention to the characteristic separation length between the filaments.

Our model of Sec. II can be easily extended to the case of an electrodeposition in the shape of rectilinear, equally spaced, parallel filaments. The system can no longer be treated as one dimensional, but the periodicity allows one to restrict the two-dimensional plane to a stripe located, for example, between a filament and the middle line between two adjacent filaments (for example if the filaments lie at $x<0$ and $y=0,\pm 2a,\pm 4a,\ldots$, the stripe can be taken as $0<y<a$). Furthermore, in a constant applied field, the filaments will grow at a constant speed, and we may expect to find a steady state in the *reference frame attached to the filament tips.* If the filaments grow at a speed $\mathbf{v}$, then the equations in the moving frame are readily deduced from (6)–(8):

$$\frac{\partial C_c}{\partial t} = D_c \Delta C_c - (\mu_c \mathbf{E} - \mathbf{v})\cdot\nabla C_c - \mu_c C_c \nabla\cdot\mathbf{E} , \tag{39}$$

$$\frac{\partial C_a}{\partial t} = D_a \Delta C_a + (\mu_a \mathbf{E} + \mathbf{v})\cdot\nabla C_a + \mu_a C_a \nabla\cdot\mathbf{E} , \tag{40}$$

$$\nabla\cdot\mathbf{E} = e(z_c C_c - z_a C_a)/\epsilon\epsilon_0 . \tag{41}$$

(It is recalled that $\mathbf{E}$ and $\mathbf{v}$ are antiparallel.) Here again these equations have been solved by numerical integration, and also a simple reasoning, based upon analytic considerations, has been worked out. In the following we will present these two treatments successively.

A. Numerical resolution

In view of the increased complexity of the problem when going from one dimension (1D) to 2D, we will first present the numerical resolution. For numerical integration of Eqs. (39)–(41), the two-dimensional domain was restricted to a rectangular box by cutting the stripe far enough from the origin, and was discretized using a square mesh of typically 100×10 points.[19] The boundary conditions were $\partial F/\partial y = 0$ $(F = C_c, C_a, V)$ for $y = a$ and for $y = 0$, $x > 0$ (symmetry axes); $\partial C_c/\partial y = 0$, $W_{ay} = 0$, $V = -(kT/z_c e)\ln(z_c C_c/C_0)$ for $y = 0$, $x < 0$ (filament); $\partial C_c/\partial x = \partial C_a/\partial x = 0$, $\partial E_x/\partial x = 0$ for $x = x_{\min}$ (boundary far inside the deposit); the boundary condition far outside the deposit was taken assuming that the electrolyte is unperturbed there ($z_c C_c = z_a C_a = C_0$, $E_x = E_0$ for $x = x_{\max}$) since the perturbations advance at the same velocity v_a as the moving front. In practice Eq. (41) was also transformed into an evolution equation

$$\frac{\partial V}{\partial t} = K'[\Delta V + e(z_c C_c - z_a C_a)/\epsilon\epsilon_0] \tag{42}$$

which was solved together with Eqs. (39) and (40) according to an explicit recursion scheme. The values of the constant K' in Eq. (42) and of the time increment in the numerical scheme were chosen for optimum convergence. [The "artificial" transformation of Eq. (41) into Eq. (42) obviously sacrifices the idea of a convergence scheme that would exactly follow the physical route toward the steady state.] The potential drop δV near the interface was taken as a parameter;[25] the velocity of the front was given an initial value v_a and was updated each recursion step in order to keep δV to the desired value. Such calculations were simple enough to be performed on a PC-type microcomputer.

Figure 4 shows some typical results. The two-dimensional maps of C_c, C_a, and V are displayed. Two

very different cases are found to occur depending upon the value of a. For values of a smaller than a critical value a_c, the electrolyte appears to be completely ion depleted behind the front of the deposit. In other words, all the metal ions are consumed by the electrodeposition process, and the velocity of the front converges to the expected value v_a (full-deposition regime). For values of a larger than a_c, part of the ions survive between the filaments; since the net anion flux through the domain is zero, this implies an advance speed larger than v_a [if α is the fraction of anions that survive between the filaments, then $\alpha v = v - v_a$, hence $v = v_a/(1-\alpha)$], which is verified by the obtained value of v (partial-deposition regime). Now it is clear that these regimes will both be unstable. The partial-deposition regime, by allowing massive penetration of the ions between the filaments, will favor branching, hence decreasing of a. On the other hand, in the full-deposition regime, any filament growing at a slightly reduced speed will die out rapidly by starving, as the ions will be consumed more efficiently by the neighboring filaments. A reasonable conclusion then is that the naturally occurring spacing must be of the order of the critical spacing $2a_c$. We have determined $2a_c$ for various sets of parameters E_0, C_0, and V_ϵ. The critical spacing $2a_c$ is found to increase with increasing δV and to decrease with increasing $|E_0|$ and C_0. However, here again only rather low values of C_0 have been usable. This has prompted us to make an analytic study of Eqs. (39)–(41), that we are going to present now. All the results will be discussed together below in more detail.

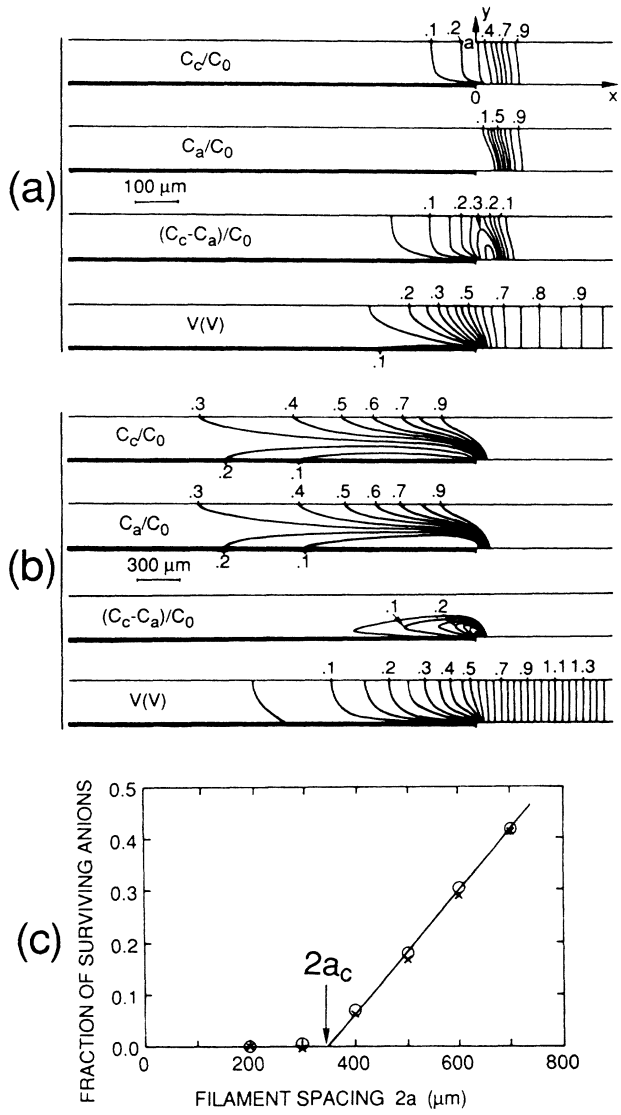

FIG. 4. Typical results for the numerical resolution of the 2D problem of filamentary growth. These are 2D maps of the ion concentrations C_c and C_a, and electrostatic potential V, in the stripe $0<y<a$, representing one half of the 2D domain between two neighboring filaments (see text). The space charge $z_cC_c - z_aC_a$ is also shown. The filaments appear as the bold segments. $E_0=10$ V/cm, $D_c=D_a=10^{-5}$ cm^2/s, $z_c=z_a=1$, $\epsilon=80$, $C_0=10^{12}$ cm^{-3}, $\delta V=0.55$ V; (a) $a=100$ μm, (b) $a=300$ μm. Notice the change of scale and also the change of behavior between (a) and (b). (c) shows, as a function of a, the fraction α of anions left at $x=x_{\min}$ (anions "leaking" through the front of the deposit), calculated from (○) the average concentration on the segment $(x_{\min}, y=0)$ to $(x_{\min}, y=a)$, and (×) the quantity $1-v_a/v$, where v is the velocity of the front. This provides a verification of the conservation of the anions $\alpha=1-v_a/v$, and gives a practical method for the determination of the critical value a_c.

B. Analytic study

The regional approximation scheme that was used in Sec. II B is not easily transposed to the two-dimensional case. This can, however, be done in the simple case where the spacing between the filaments is infinitely small, since the problem then turns back to one dimensional. We will first present this calculation, then we will analyze what occurs upon increasing a.

1. *Case of infinitely small spacing*

In the case of vanishingly small a, the problem becomes one dimensional. It is, however, slightly different from the problem of Sec. II because of the motion of the reference frame and different boundary conditions, here $dC_c/dx(0)=0$, $W_a(0)=0$, $V(0) = -(kT/z_ce)\ln[z_cC_c(0)/C_0]$. Taking $v=v_a$, Eqs. (39)–(41) reduce to

$$D_c\frac{d^2C_c}{dx^2}+\mu_c\frac{d}{dx}\left[C_c\frac{dV}{dx}\right]+v_a\frac{dC_c}{dx}=0\ , \tag{43}$$

$$D_a\frac{d^2C_a}{dx^2}-\mu_a\frac{d}{dx}\left[C_a\frac{dV}{dx}\right]+v_a\frac{dC_a}{dx}=0\ , \tag{44}$$

$$d^2V/dx^2=-e(z_cC_c-z_aC_a)/\epsilon\epsilon_0\ . \tag{45}$$

These equations are very similar to Eqs. (12)–(14) and their resolution can be carried out in the same way as in Sec. II B. Integration of Eqs. (43) and (44) gives

$$-D_cdC_c/dx-\mu_cC_cdV/dx-v_aC_c=(\mu_c+\mu_a)E_0C_0/z_c\ , \tag{46}$$

$$-D_adC_a/dx+\mu_aC_adV/dx-v_aC_a=0\ , \tag{47}$$

which are similar to Eqs. (17) and (15), respectively. Equation (47) can be further integrated to

$$C_a(x) \propto \exp[z_a e V_a(x)/kT] \tag{48}$$

with

$$V_a(x) = V(x) + E_0 x \ . \tag{49}$$

Following the same scheme as in Sec. II B, and starting from $x = x_{\max}$, one again finds two regions: *(i) Quasineutral region:*

$$z_c C_c \approx z_a C_a$$

$$\approx C = C_0 \left[1 - \exp \left[(1+\mu_a/\mu_c) \frac{z_c z_a}{z_c + z_a} \times \frac{eE_0}{kT}(x - x_1) \right] \right] , \tag{50}$$

$$V = \delta V - E_0 x + (kT/z_a e) \ln(C/C_0) \ ; \tag{51}$$

(ii) space-charge region, for

$$x < x_1 = \left[\frac{9\epsilon\epsilon_0 \delta V^2}{-8eE_0 C_0 (1+\mu_a/\mu_c)} \right]^{1/3} ,$$

(notice that x_1 bears some similarity with x_I of Sec. II)

$$C_a \ll C_c \approx \left[-\frac{\epsilon\epsilon_0 E_0 C_0 (1+\mu_a/\mu_c)}{2z_c^2 e (x_1 - x)} \right]^{1/2} , \tag{52}$$

$$V = V(0) + [\delta V - V(0)][1 - (1 - x/x_1)^{3/2}] , \tag{53}$$

where $V(0)$ is given by

$$V(0) = \frac{kT}{z_c e} \ln \left[\frac{3e\delta V C_0}{\epsilon\epsilon_0 E_0^2 (1+\mu_a/\mu_c)^2} \right]^{1/3} . \tag{54}$$

The resulting solution is represented in Fig. 5. There is an obvious analogy with Fig. 2. Actually the present solution can be obtained from Eqs. (32)–(38) by simple substitution of V_0 by δV and $L/2$ by the backstream diffusion length $\lambda_b = (-kT/eE_0)(z_c + z_a)[z_c z_a (1+\mu_a/\mu_c)]^{-1}$. Here, however, a truly neutral region is present ahead of the quasineutral region, i.e., for $x > x_1 + \lambda_b$, where the applied electric field survives, and a most important parameter δV appears, which represents essentially the potential drop in the space-charge region. This δV of course should depend upon the microscopic mechanism giving rise to the surface instability (the more unstable the surface, the smaller δV). Here we will not attempt such a microscopic theory and keep δV as a parameter. A noteworthy feature is the role of δV in connection with anion depletion: δV is generated by the positive charge left upon anion depletion; on the other hand [see Eq. (48)], the anion concentration appears to be in equilibrium in the moving frame in a potential $V_a = V + E_0 x$, i.e., there is no effective force exerted on the anions in the neutral region, but the energy $z_a e \delta V$ appears as a potential barrier that prevents them from entering the region $x < x_1$. This point of view will be very useful for giving insight into the problem of an arbitrary filament spacing.

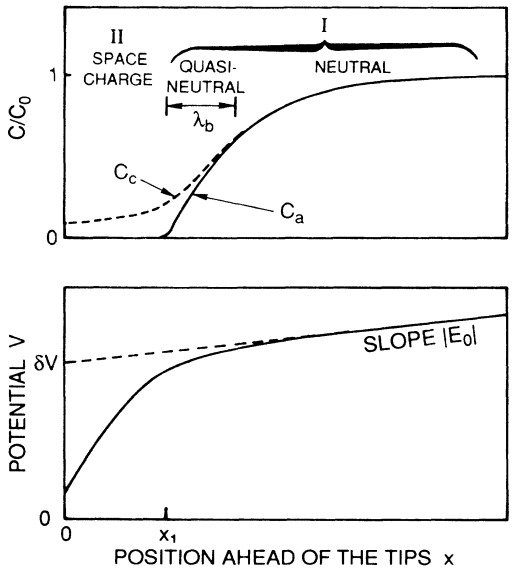

FIG. 5. Profiles of the ion concentrations C_c and C_a, and electrostatic potential V in the moving frame, in the case of filamentary growth with an infinitely small spacing between the filaments. The same two regions as in Fig. 2 can be found. Notice, however, the appearance of a truly neutral region ahead of the quasineutral region, i.e., for $x - x_1 \gg \lambda_b$.

Also, in an experiment, it is clear that this potential drop δV will reach its steady-state value only after some time, corresponding to building up of the space charge. This time is a natural explanation for the induction time before ramified growth, which has been observed experimentally.[17,24]

2. *Arbitrary filament spacing*

For filament spacings larger than x_1, the problem of Eqs. (39)–(41) is really two dimensional and the above approximation breaks down. However, Eq. (40) can be written

$$\nabla \cdot (-D_a \nabla C_a + \mu_a C_a \nabla V - \mathbf{v}_a C_a) = 0 \ . \tag{55}$$

In the case where no anions can penetrate the $x < 0$ region, and in view of the boundary conditions, the sum of the terms in parentheses can itself be deduced to be zero (this is just $\mathbf{W}_a$ in the moving frame), hence

$$C_a(x,y) \propto \exp[z_a e V_a(x,y)/kT] \tag{56}$$

with

$$V_a(x,y) = V(x,y) + E_0 x \ , \tag{57}$$

which is just the 2D extension of Eqs. (48)–(49). The crucial point then is to predict whether or not the effective potential $V_a = V + E_0 x$ will be able to prevent the anions from reaching the $x < 0$ region. In the absence of any space-charge effects, V would be simply given by solving the 2D Laplace equation with a metallic comb as the boundary condition. Such a potential, schematized in Fig. 6(a), will clearly oppose a barrier to anion penetra-

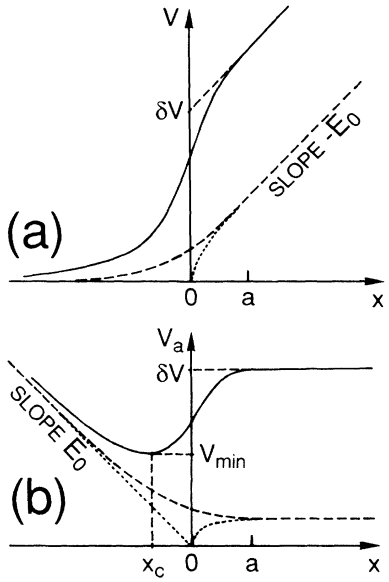

FIG. 6. Electrostatic potentials as a function of x: (a) electrostatic potential V in the absence of space charge, with an applied electric field E_0 [represented along $y=0$ (dotted line) and along $y=a$ (dashed line)], and in the presence of a positive space charge near the filament tips (solid line, shown along $y=a$); (b) same for the effective potential $V_a=V+E_0x$ seen by the anions in the moving frame. a and δV have been chosen in the full-deposition regime ($a<a_c$). Notice the appearance of a potential barrier ($\delta V>V_{\min}$) preventing the anions from reaching the $x<x_c$ region. For $\delta V<V_{\min}$ the barrier disappears and the ions massively penetrate between the filaments. In this figure, for clarity, the Nernst contribution $V(0)=(-kT/z_ce)\ln[z_cC_c(0)/C_0]$ has been assumed to be negligible.

tion along $y=0$, but no barrier along $y=a$ [see Fig. 6(b)]. Deviations from electroneutrality are therefore of primary importance in creating a barrier against anion penetration. Such deviations occur of course in the space-charge region, but also in the quasineutral region [see Eq. (51)]. Depending upon the values of x_1 and λ_b, either of these regions may govern the appearance of the potential barrier. Namely, for extremely dilute electrolytes, one would have $x_1\gg\lambda_b$ and the space-charge region might play the dominant role; on the other hand, for more realistic concentrations, one will have $x_1\ll\lambda_b$, the space-charge region will penetrate between the filaments, and the critical spacing will be determined by the quasineutral region. Only the latter regime is of interest for the practical case. However, because the numerical calculations are actually performed in the intermediate regime, we will successively consider the two regimes in the following, then we will discuss the obtained results.

(a) Dilute regime: space-charge region dominant. For very dilute concentrations ($C_0/E_0^2\ll10^{12}$ cm^{-1}V^{-2}), Eqs. (50)–(53) give $x_1\gg\lambda_b$. Then if the space-charge region can fully penetrate between the filaments, the bulk ion concentrations will also penetrate (partial-deposition regime). In other words, the space-charge region is the only defense against penetration of the ions between the filaments. We then consider the case where the quasineutral region stays ahead of the filament tips, and focus on the space-charge region.

The space charge is expected to be maximum near the filament tips. For small filament spacings, the space-charge regions associated with neighboring filaments overlap, so that there is a potential barrier opposing ion penetration for all the values of y (including $y=a$). Vanishing of the potential barrier for $y=a$ is expected to occur when the filament spacing becomes large enough so that neighboring space-charge regions no longer overlap. For a qualitative estimate of the critical spacing, one may model the space-charge region associated with a filament tip as a roughly disk-shaped domain, with a cation concentration C_c. The critical spacing will just occur when a is of the order of magnitude of the radius of this domain.

Now electrostatics and current conservation impose two conditions, which allow us to determine C_c and a. (i) The potential drop δV can be related to the equivalent dipoles formed by the positive space charges and negative counterchanges on the filaments. Since each dipole is of typical magnitude $ez_cC_aa^3$ and the linear dipole density is $\sim1/a$, then one has

$$\delta V\sim ez_cC_ca^2/\epsilon\epsilon_0\ . \tag{58}$$

(This is an approximate integral version of the Poisson equation.) (ii) The typical electric field in the space-charge region is $\sim\delta V/a$, hence the total current driven to a given filament is $\sim(ez_c\mu_cC_c)(\delta V/a)a$. The sum over all filaments must equal the current far ahead of the front, hence

$$ez_c\mu_cC_c\delta V/a\sim-eC_0(\mu_c+\mu_a)E_0\ . \tag{59}$$

Eliminating C_0 between Eqs. (58) and (59), one gets the critical value for a,

$$a_c\sim[-\epsilon\epsilon_0\delta V^2/eE_0C_0(1+\mu_a/\mu_c)]^{1/3}\ . \tag{60}$$

As one might have expected it, this value of a_c is just of the order of magnitude of x_1.

(b) Practical regime: quasineutral region dominant. For more realistic concentrations ($C_0/E_0^2\gg10^{12}$ cm^{-1}V^{-2}), Eqs. (50)–(53) give $x_1\ll\lambda_b$. Then if $a>x_1$ the space-charge region may penetrate along the filaments; but the penetration of the bulk electrolyte will still be hindered as long as λ_b stays larger than a. We are thus going to examine the 2D behavior of the quasineutral region in more detail.

Figure 7 shows the expected map of the various regions in the full-deposition regime. The quasineutral region penetrates between the filaments, and is separated from the filaments by a thin space-charge layer. It is limited, on the $x<0$ side, by a small space charge similar to that calculated above. As long as we are in the full-deposition regime, the anions are in equilibrium in the moving frame, and we can use Eqs. (56) and (57) in Eq. (39), hence

$$-D_c(1+z_c/z_a)\Delta C+(\mu_c+\mu_a)E_0\frac{\partial C}{\partial x}=0\ . \tag{61}$$

As long as the space-charge-layer thickness is much smaller than a, this equation can be solved with the

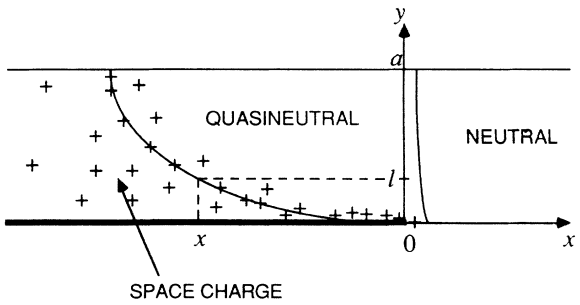

FIG. 7. Scheme of the various regions for 2D growth in the moving frame, in the case of practical concentrations ($C_0/E_0^2 \gg 10^{12}$ cm^{-1} V^{-2}). The plus signs stand for the positive charges in the space-charge region.

boundary condition $C_c(x,0)=0$ (here we make use of the fact that the concentration in the space-charge region is much smaller than C_0), and a solution of the form $F(x)\sin(\pi y/2a)$ may be looked for. The result is (with $C \approx z_c C_c \approx z_a C_a$)

$$C(x,y)=C_0 \sin(\pi y/2a)\exp(x/\lambda_{\text{eff}}) \tag{62}$$

with

$$\lambda_{\text{eff}}=2[(\lambda_b^{-2}+\pi^2 a^{-2})^{1/2}-\lambda_b^{-1}]^{-1} \tag{63}$$

and

$$\lambda_b=(-kT/eE_0)(z_c+z_a)[z_c z_a(1+\mu_a/\mu_c)]^{-1} . \tag{64}$$

The concentration of the electrolyte is found to decrease exponentially upon penetrating between the filaments. The effective anion potential also decreases, according to Eqs. (56) and (57). This provides the barrier against anion penetration. The simple regime depicted by Eq. (61) will end for x negative enough so that the space-charge-layer thickness l reaches the same order of magnitude as a ("pinch off" of the quasineutral region). An estimate of l requires consideration of the space-charge layer. This can be done in a 1D approximation, taking into account only the dependences along y:

$$V=V(x,0)+[\delta V-E_0 x-V(x,0)][1-(1-y/l)^{3/2}] , \tag{65}$$

$$C_c=C_s(1-y/l)^{-1/2} . \tag{66}$$

Writing the boundary condition at (x,l)

$$J_y=-eD_c C(\pi/2a)(1+z_c/z_a) \tag{67}$$

and using the Poisson equation finally yields [with the assumption $V(x,0) \ll \delta V$]

$$C_s \approx C\frac{\pi kT(1/z_c+1/z_a)l}{3z_c ea(\delta V-E_0 x)} \approx \frac{3\epsilon\epsilon_0(\delta V-E_0 x)}{4z_c el^2} . \tag{68}$$

Hence

$$l^3 \approx \frac{9\epsilon\epsilon_0}{4\pi}\frac{a(\delta V-E_0 x)^2}{kTC(1/z_c+1/z_a)} . \tag{69}$$

In view of the variation of C, given by Eq. (62), the maximum of l will be reached for

$$x=2\lambda_{\text{eff}}+\delta V/E_0 . \tag{70}$$

In practice, even if the corresponding value of l stays smaller than a, one will consider that an efficient defense against ion penetration is reached if, at this position, the initial concentration has dropped to a small fraction of its initial value, say $\alpha \sim 10^{-1}-10^{-2}$. This gives the condition

$$x < \lambda_{\text{eff}} \ln\alpha . \tag{71}$$

Hence from Eqs. (63) and (70)

$$2a_c \sim 2\pi(2q/\lambda_b+q^2)^{-1/2} \tag{72}$$

with

$$q=2(2-\ln\alpha)|E_0|/\delta V \tag{73}$$

and λ_b as given by Eq. (64).

C. Discussion

Equations (60) and (72) provide two determinations for the value of the critical spacing $2a_c$ at which the transition between the full-deposition and partial-deposition regimes occurs. We recall that this is expected to be the natural spacing occurring between the growing filaments. These two predictions have been represented in Figs. 8 and 9 as the curves, together with the values of $2a_c$ obtained from the numerical resolution of Eqs. (39)–(41). As expected, the numerical results for the lowest concentration (10^{11} cm^{-3}) are rather close to the prediction

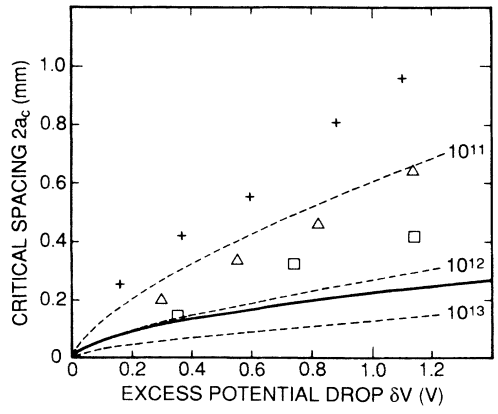

FIG. 8. The critical value $2a_c$, representing the prediction for the natural spacing between the filaments, as a function of δV, from the numerical calculations. $D_c=D_a=10^{-5}$ cm^2/s, $z_c=z_a=1$, $\epsilon=80$, $E_0=-10$ V/cm; +, $C_0=10^{11}$ cm^{-3}; △, $C_0=10^{12}$ cm^{-3}; □, $C_0=10^{13}$ cm^{-3}. The curves have been obtained from Eqs. (60) and (74), representing the two extreme concentration regimes (dashed curves for the low concentrations [Eq. (60)], and solid curve for practical concentrations [Eq. (74)]). Notice the crossover between 10^{12} and 10^{13} cm^{-3}. The numerical results, obtained in the intermediate regime, can best be represented as the sum of these two contributions.

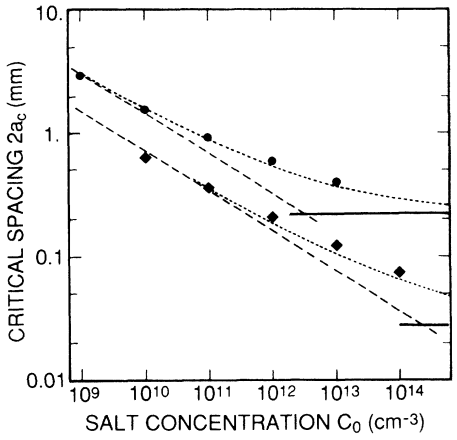

FIG. 9. The critical value $2a_c$, representing the prediction for the natural spacing between the filaments, as a function of C_0, from the numerical calculations. $D_c=D_a=10^{-5}$ cm^2/s, $z_c=z_a=1$, $\epsilon=80$; ●, $E_0=-10$ V/cm, $\delta V=1.1$ V; ◆, $E_0=-100$ V/cm, $\delta V=1.5$ V. The curves have been obtained from Eqs. (60) and (74), representing the two extreme concentration regimes (dashed curves for the low concentrations [Eq. (60)], and solid curves for practical concentrations [Eq. (74)]). Notice the crossover concentration, scaling as E_0^2. The dotted curves represent the sum of the two contributions from Eqs. (60) and (74).

from Eq. (60). For increasing values of C_0/E_0^2, the calculated points become increasingly closer to the prediction from Eq. (72). A rather accurate description of the numerical results would actually be obtained as the sum of the two contributions from Eq. (60) and (72) (see dotted curves in Fig. 9). This can be understood easily: since the space-charge region and quasineutral region both act as a defense against ion penetration between the filaments, the approximate additivity of their effects may indeed be expected. We will now consider in more detail the high-concentration regime, which is that encountered in practice ($C_0\sim10^{18}-10^{20}$ cm^{-3}). Our prediction for experimental situations can then be given more explicitly from Eq. (72),

$$2a_c\approx\frac{\pi}{2-\ln\alpha}\frac{\delta V}{|E_0|}\times\left[1+\frac{e\delta V}{(2-\ln\alpha)kT}\frac{z_cz_a}{z_c+z_a}(1+\mu_a/\mu_c)\right]^{-1/2}, \quad (74)$$

where a reasonable value for α may be $\sim10^{-1}-10^{-2}$, hence $2-\ln\alpha\sim5$. The logarithm makes the order of magnitude of $2a_c$ rather insensitive to the exact choice for α.

One will notice that this value is somewhat larger than λ_b, by a factor $\sim(e\delta V/kT)^{1/2}$. (This corrective factor makes the high-concentration regime attained for concentrations appreciably below the above given nominal condition $\lambda_b\gg x_1$.) For large enough δV, the critical spacing $2a_c$ from Eq. (74) is proportional to $\delta V^{1/2}$ and inversely proportional to $|E_0|$. Comparison with experiment would of course require the measurement of δV. An experiment has indeed been performed, where the potential of the electrolyte was probed with a series of copper-wire probes, giving access to the full potential distribution through the cell.[17] From this measurement, values of $\delta V\sim3$ V can be deduced, and the predicted values $2a_c\sim0.5$ mm from Eq. (74) are in fair agreement with the experimental measurements. However, a systematic study of $2a_c$ as a function of δV and $|E_0|$ is still to be performed.

More detailed predictions on the morphology of the filaments can also be extracted from the above calculation [Eqs. (61)–(73)]. The observed filaments are actually known to be covered with small sidebranches. The average angle θ between the sidebranches and the filament axis can be predicted from the ratio of the x and y components of the cation current in the laboratory frame:

$$\tan\theta=\frac{J_{cy}}{J_{cx}}=\cot\left[\frac{\pi y}{2a}\right]\frac{\pi/2a}{1/\lambda_{\text{eff}}-(eE_0/kT)z_cz_a/(z_c+z_a)}. \quad (75)$$

Using Eqs. (70)–(73), one finally obtains

$$\tan\theta=\cot\left[\frac{\pi y}{2a}\right]\times\frac{\left[1+\frac{e\delta V}{(2-\ln\alpha)kT}\frac{z_cz_a}{z_c+z_a}\left[1+\frac{\mu_a}{\mu_c}\right]\right]^{1/2}}{\left[1+\frac{e\delta V}{(2-\ln\alpha)kT}\frac{z_cz_a}{z_c+z_a}\right]}. \quad (76)$$

Taking $\cot(\pi y/2a)\sim1$ and $e\delta V\gg kT$, this gives the prediction $\tan\theta\sim(20kT/e\delta V)^{1/2}$. It is interesting to consider this prediction in parallel with the prediction for the average filament spacing: if the applied electric field $|E_0|$ is *decreased*, a decrease of δV is to be expected. The average spacing depends most strongly on $|E_0|$ and will then *increase*. The average angle is governed by δV and will *increase*. This seems to describe a *progressive* transition from the "dense-branched" to the "DLA" morphology. To this point one might even question whether the "DLA"regime may exist at all, except as an asymptotic limit when the applied field is made vanishingly small.

An appealing work, of course, would be an investigation of the microscopic mechanism responsible for the appearance of δV. A first naive guess might be that ramified growth will occur as soon as the deposition rate will overwhelm surface diffusion in the vicinity of the filament tips. However, various problems will have to be addressed: since each filament is actually ramified, it exhibits multiple tips; also, the dependence of equilibrium potential upon interface curvature, the interface overpotential, and the convection in the electrolyte, which have been completely neglected here, might well play an important role in practice. This is especially true for convection, which indeed seems to be present in the experiments.[24] These problems will probably make deeper in-

vestigations increasingly difficult. Yet the role of δV in governing the morphological transitions might be very important and would deserve further analysis. Further work trying to incorporate electrolyte convection is presently being planned.

IV. CONCLUSION

We have shown that the growth of ramified metallic electrodeposits in dilute salt solutions is essentially driven by the space charge that tends to develop upon anion depletion near the cathode. The front of the ramified electrodeposit has been shown to advance at a velocity $v_a = -\mu_a E_0$, which is just the velocity of the anions, determined by their mobility μ_a and the electric field E_0 in the neutral region of the electrolyte. We have further shown that the same kind of analysis can be fruitfully applied to the growth in the dense-parallel morphology: it is shown that there is a space-charge region concentrated near the tips of the growing filaments, with an associated potential drop δV; the characteristic time for building the space charge gives a natural explanation for the observed induction time before beginning of the growth, the average filament spacing is predicted to be of the order of $(\delta V kT/eE_0^2)^{1/2}$, and the average sidebranch tilting angle of the order of $(20kT/e\delta V)^{1/2}$, in qualitative agreement with experiment. These trends are highly suggestive of a progressive transition from the "dense-branching" morphology to the "DLA" morphology as the electric field E_0 is reduced.

ACKNOWLEDGMENTS

This work is largely the result of the friendly stimulation, numerous discussions, and the constant interest of V. Fleury, M. Rosso, and B. Sapoval. The author is also indebted to Dr. G. Maurin for useful disscussions, and especially for bringing some valuable references to his attention. The Laboratoire de Physique de la Matière Condensée is "Unité de Recherche Associée 1254 du Centre National de la Recherche Scientifique."

[1] J. L. Barton and J. O'M. Bockris, Proc. R. Soc. London, Ser. A **268**, 485 (1962).

[2] R. M. Brady and R. C. Ball, Nature (London) **309**, 225 (1984).

[3] M. Matsushita, M. Sano, Y. Hayakawa, H. Honjo, and Y. Sawada, Phys. Rev. Lett. **53**, 286 (1984).

[4] D. Grier, E. Ben-Jacob, R. Clarke, and L. M. Sander, Phys. Rev. Lett. **56**, 1264 (1986).

[5] D. G. Grier, D. A. Kessler, and L. M. Sander, Phys. Rev. Lett. **59**, 2315 (1987).

[6] F. Argoul, A. Arneodo, G. Grasseau, and H. L. Swinney, Phys. Rev. Lett. **61**, 2558 (1988).

[7] D. B. Hibbert and J. R. Melrose, Phys. Rev. A **38**, 1036 (1988).

[8] G. L. M. K. S. Kahanda and M. Tomkiewicz, J. Electrochem. Soc. **136**, 1497 (1989).

[9] P. Garik, D. Barkey, E. Ben-Jacob, E. Bochner, N. Broxholm, B. Miller, B. Orr, and R. Zamir, Phys. Rev. Lett. **62**, 2703 (1989).

[10] A. R. Despić and K. I. Popov, in *Modern Aspects of Electrochemistry,* edited by B. E. Conway, and J. O'M. Bockris (Plenum, New York, 1972), Vol. 7, pp. 199–313.

[11] P. Fedkiw, J. Electrochem. Soc. **127**, 1304 (1980).

[12] R. Aogaki, K. Kitazawa, Y. Kose, and K. Fukei, Electrochim. Acta **25**, 965 (1980).

[13] D. P. Barkey, R. H. Muller, and C. W. Tobias, J. Electrochem. Soc. **136**, 2207 (1989).

[14] J. Newman, Trans. Faraday Soc. **61**, 2229 (1965).

[15] W. H. Smyrl and J. Newman, Trans. Faraday Soc. **63**, 207 (1967).

[16] N. Ibl, in *Comprehensive Treatise of Electrochemistry,* edited by E. Yeager, J. O'M. Bockris, B. E. Conway, and S. Sarangapani (Plenum, New York, 1983), Vol. 6, pp. 39–43.

[17] V. Fleury, J.-N. Chazalviel, M. Rosso, and B. Sapoval, J. Electroanal. Chem. **290**, 249 (1990).

[18] J. O'M. Bockris and A. K. N. Reddy, *Modern Electrochemistry* (Plenum, New York, 1970), Vol. 1, Chap. 4.

[19] One might question the validity of using the 2D version of the Poisson equation ($\Delta V = \partial^2 V/\partial x^2 + \partial^2 V/\partial y^2$, with $\partial^2 V/\partial y^2 = 0$ in the 1D case). This implies that the electric field stays confined between the two parallel plates limiting the cell. This is indeed a fair approximation in view of the very large dielectric constant of water as compared to that of the plates, which are usually made of glass: using high-dielectric-constant plates for the cell walls might affect the validity of this approximation, hence possibly the morphology of the deposits. Also, in the growth regime where the metal deposit grows right against the cell wall (V. Fleury, unpublished), the breakdown of this approximation is to be expected.

[20] The interface boundary condition is equilibrium of the *electrochemical* potential, not of the *electrostatic* potential. The electrostatic potential in the electrolyte V' therefore differs from that of the electrode V, namely, $V' = V + (U_{PZC} - U_{equ})$, where U_{PZC} and U_{equ} are the electrode potentials corresponding to zero charge and electrochemical equilibrium, respectively. U_{equ} depends upon cation concentration according to Nernst law $U_{equ} = U_0 + (kT/z_c e)\ln(z_c C_c/C_0)$ hence $V' = V + (U_{PZC} - U_0) - (kT/z_c e)\ln(z_c C_c/C_0)$. We will drop the constant term $U_{PZC} - U_0$ in the following. This amounts to choosing a different origin for the electrostatic potential when in the electrolyte.

[21] See, e.g., F. John, *Lectures on Advanced Numerical Analysis* (Gordon and Breach, New York, 1967), Chap. 6, pp. 110–113.

[22] R. Bruinsma and S. Alexander, J. Chem. Phys. **92**, 3074 (1990).

[23] Same as Ref. 18, Vol. 2, Chap. 9, pp. 1050–1052.

[24] V. Fleury (unpublished).

[25] Since we had inferred earlier that one should have $v = v_a$, it was tempting to constrain v to this value, and investigate the steady state for various spacings between the filaments. We have found that this constraint leads to an undetermination of the steady state. One must instead fix a condition for the growth, mimicking the physical process, and adjust the growth speed so that this condition will be satisfied. Such a reasonable condition for filament growth may consist in fixing some critical value, for example, for the electric field at

the interface, or else for the potential drop δV in the vicinity of the interface. In practice, we have found it most convenient to adjust the growth speed so that the potential $V(0,a)$ be equal to some value V_ϵ. [Actually it turns out that in the steady state $V(0,a)$ is about identical to δV, but convergence is more easily achieved by fixing $V(0,a)$.] The speed v of the front was initialized to v_a, and was corrected at each step n by looking at the deviation δ of $V(0,a)$ from the required value V_ϵ, and taking $v_n = v_{n-1}(1+\alpha_1\delta)$. An improved convergence speed was obtained by adding a multiplicative correction $(1-\alpha_2\delta)$ to the potential $V(x,y)$. (α_1 and α_2 are constants whose values determine the convergence speed).